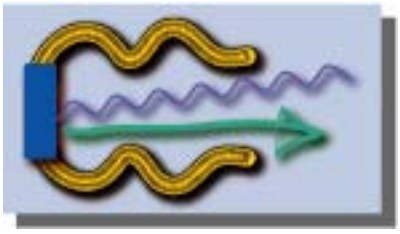

PHIN

Design of a RF Photo-Gun

R. Roux, G. Bienvenu, C. Prevost, B. Mercier, *LAL-Orsay*

We acknowledge the support of the European Community-Research Infrastructure Activity under the FP6 “Structuring the European Research Area” programme (CARE, contract number RII3-CT-2003-506395).

Design of a RF Photo-Gun

Contributors: R. Roux, G. Bienvenu, C. Prevost, B. Mercier (LAL-Orsay)

LAL is involved in WP4 of JRA2 (PHIN) through the design and construction of a radio-frequency gun for the CLIC Test Facility 3 (CTF3) at CERN. The design study of the gun began in January, 2004. This gun is based on a previous proto-type CERN RF gun (so called "type IV"). However, it needs further study in order to meet the specifications of the CTF3 photo-injector (see table 1).

RF frequency (GHZ)	2.99855
RF power (MW)	30
Beam energy (MeV)	5 – 6 MeV
Beam current (A)	3.51
Charge/bunch (nC)	2.33
Bunch length (ps)	10
Energy spread (%)	< 2
Normalized emittance (πmmmrad)	< 25
Pulse train duration (μs)	1.548
Vacuum pressure (mbar)	2.10^{-10}

Table 1: Beam and RF gun parameters desired for CTF3.

In part one of this report we show the results of the RF simulations performed with a 2-D electromagnetic code, SUPERFISH, and a 3-D code, HFSS, which allowed us to obtain the main characteristics such as the cavity dimensions and the axial field distribution. In the second part, simulations of the beam dynamics in the gun with the PARMELA code are summarised. In part three, we provide some calculations of the beam-loading, i.e. the voltage induced by the beam itself inside the gun, which can severely limit the gun performance. In addition, vacuum aspects have been thoroughly investigated (part four) as, in previous experiments with RF photo-injectors at CERN the pressure has been found to increase dramatically at high levels of extracted charge (≈1 μC). Finally, a preliminary schematic version of the RF gun will be shown and the expected vacuum level will be discussed.

1. RF Simulations of the Gun

These simulations are used essentially to determine the physical dimensions of the photo-injector cavity. The latter will be derived from the 2-1/2 cell RF gun which was built

and tested with beam at CERN. A schematic drawing is shown in Fig. 1. First, the main objectives are to check if this design is compatible with the CTF3 parameters. We have studied, for example, the influence of the angle of the cathode wall as well as the shape of the iris. Of course, any change to the cavity must be compensated in order to keep the resonant frequency at the required value. As this exercise can imply numerous simulations it is usual to begin by using a 2D code such as SUPERFISH especially when the structure has a cylindrical symmetry because it allows a considerably saving in time. A 3D code, HFSS, was then used to adapt two RF couplers to the gun this being impossible with SUPERFISH.

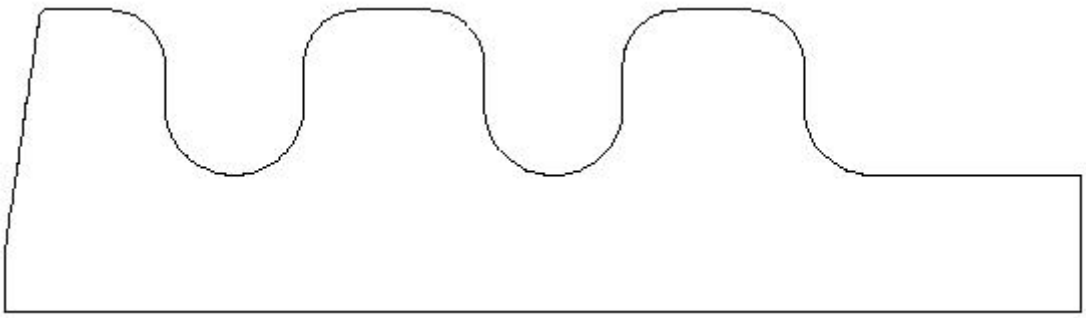

Figure 1: Schematic of the CERN type IV photo-gun.

1.1 SUPERFISH simulations

The CERN design of the RF gun was optimised for higher charge by choosing the angle of the half-cell wall, around the photo-cathode, to provide additional transverse focusing. According to dynamical calculations (see 2.1), this angle should be reduced to 3.4 ° rather than the previous value 8° in order to keep the energy spread within the desired limits.

Moreover, we have changed the shape of the iris from circular to elliptical to decrease the surface electric field and therefore it minimize electrical breakdown and dark current levels. Furthermore, we introduced a slight asymmetry in the walls of the cavities for mechanical reasons and to try to reduce multipacting hazards. The new design is shown in schematically in Fig. 2.

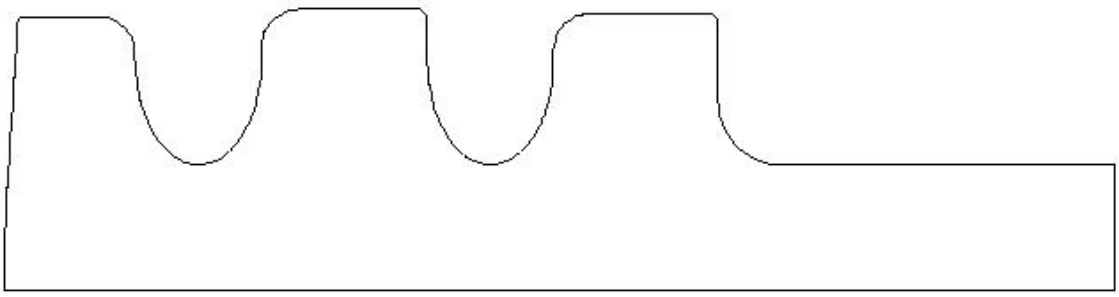

Figure 2: Schematic of the new RF Gun.

The evidence of the efficiency of the elliptical iris for the reduction of the surface electric field with respect to the circular one is illustrated in Fig. 3. At first sight, the gain is not obvious since the average field is roughly the same in the two cases. But the peak electric field in the elliptical design is 15 % lower with respect to the circular case. Now, the yield of electrons by the cavity walls by field emission is strongly non linear with the electric field. Therefore the use of the elliptical iris should be helpful for the reduction of discharge problems due to field emission.

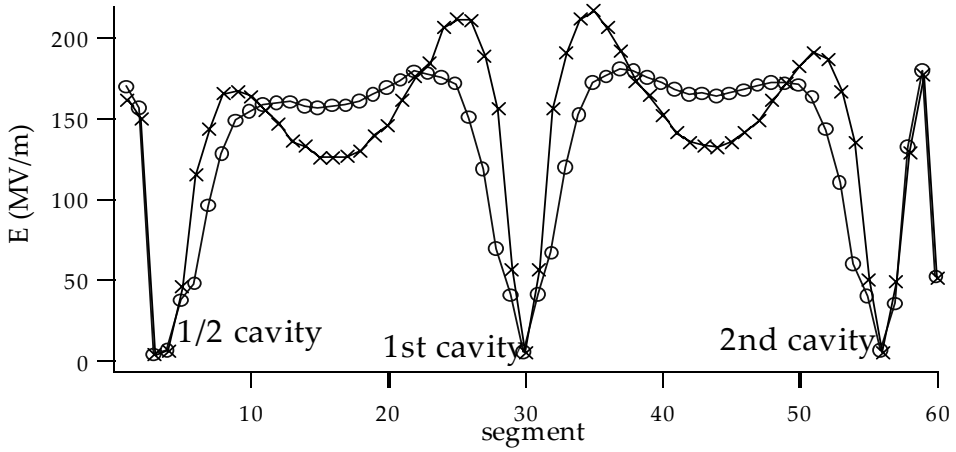

Figure 3: Surface electric field as a function of the SUPERFISH segment on the circumference of the model in figure 2. The surface electric field is zero in the mid-cells and maximum on the iris. The curve with circles shows the elliptical iris case and the curve with crosses shows the circular iris case. The axial electric field is 85 MV/m.

The parameters of this RF gun are shown in table 2. Finally, the main difficulty in designing the gun is to obtain a good axial electric field "flatness" in every cell of the structure. This requirement is rather difficult to meet as the cells are strongly coupled and any change in the radius of one cell induces a variation of the electric field in every cell. The best adjustment we have obtained is shown in Fig. 4.

Resonance frequency (GHz)	3.003052
Shunt impedance R_s (MΩ)	6
Quality factor Q	14530

Table 2: RF photo-gun parameters.

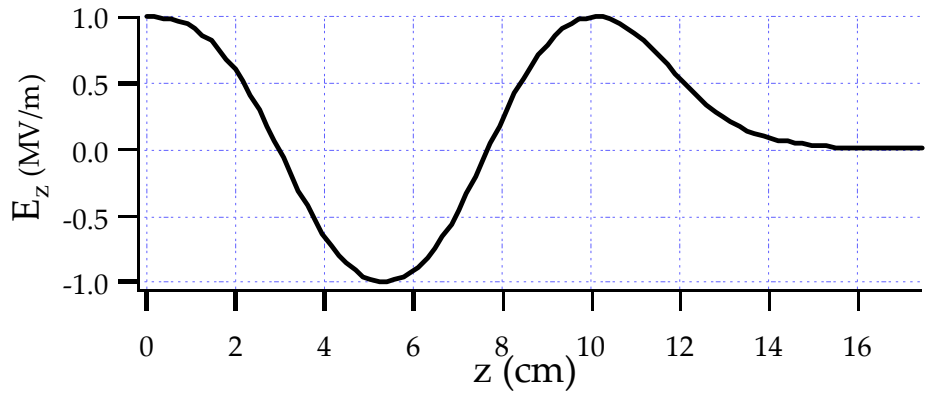

Figure 4: Axial electric field of the RF photo-gun.

1. 2 HFSS simulations

The RF power is transported to the photo-gun via wave-guides and enters the gun through coupling holes whose aperture must be adjusted to, in principle, minimise the reflected power. However, in our case, the high level of power extracted by the electron beam leads to a dramatic decrease of the coupling and therefore to enhanced reflected power. Consequently, it was decided to design the coupling factor, β, to be 2.9 which will allow the gun to be at critical coupling in the presence of a beam at the nominal current of 3.51 A. Moreover, for beam emittance preservation, the electric field must be kept symmetric around the axis. Consequently we decided to connect two couplers symmetrically with respect to the horizontal plane. The 3-D design is shown in Fig. 5.

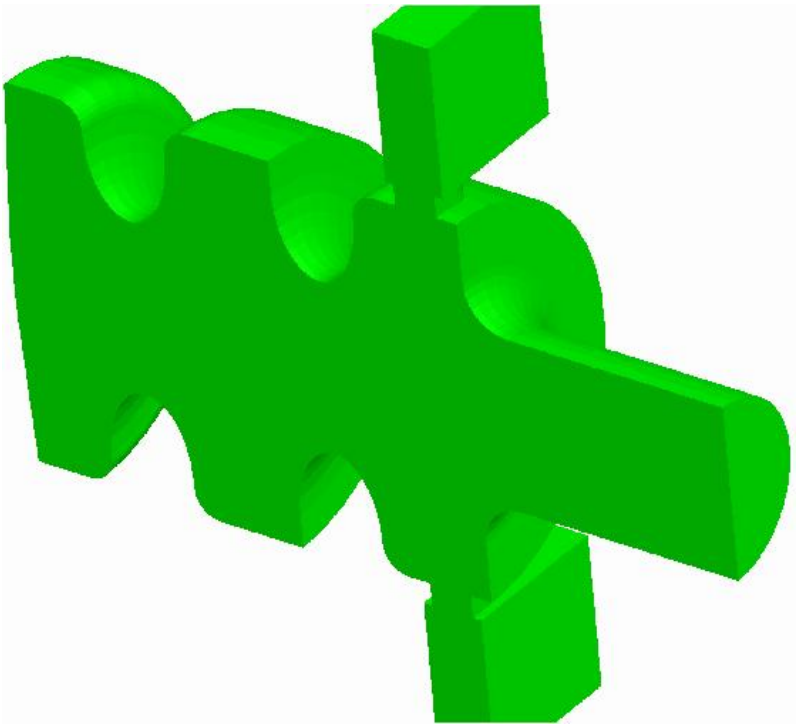

Figure 5: Half view of 3-D model of the RF photo-gun.

To leave enough space to install a solenoidal coil around the gun it was decided to connect the couplers to the output cell and to use wave-guides whose inner height is 14 mm rather than the standard 34 mm. The shape of the coupling aperture is in the form of a racetrack and its dimensions are approximately 25mm x 10mm.

In HFSS and SUPERFISH one has the possibility to obtain the eigen-modes of the structure. The results for the accelerating mode are as follows:

F_r = 3009.8 MHz

R_s = 5.92 MΩ

Q_0 = 14370

However, the most interesting feature of the HFSS code is its ability to calculate the reflected and transmitted power propagating through the structure from which the coupling is derived. The coefficients of the scattering matrix, S_{11} and S_{21}, are shown in figure 6.

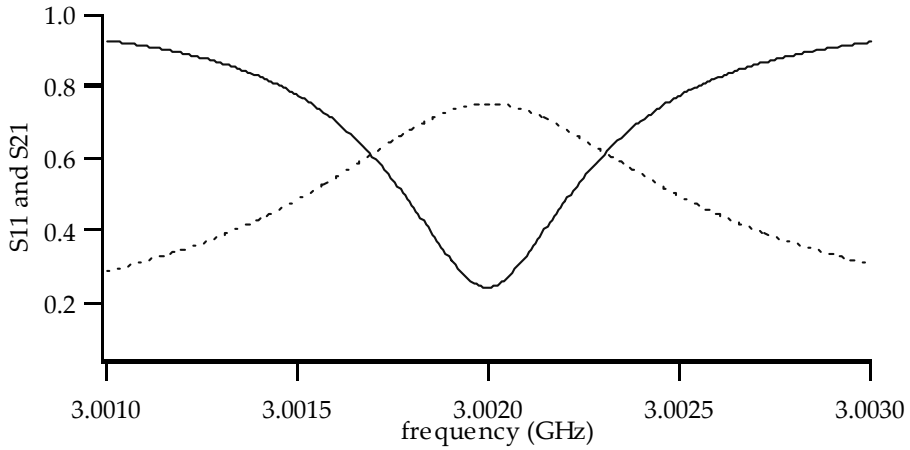

Figure 6: Full curve - S_{11}, dashed line - S_{21}, as a function of frequency.

The resonant frequency is 3.002 GHz, the difference with respect to the eigen-mode calculation is due to the opening of the cavity by the coupling apertures which decreases the frequency and the magnitude of the electric field in the last cell. This last model was obtained after many simulations since three conditions need to be satisfied in simultaneously: the resonant frequency, the coupling and the field-flatness. For instance, according to the simulations it is necessary to have the radius of the last cell 1 mm smaller than in the second cell. The equilibrium of the electric field in all directions is rather good as is shown in figure 7. The peak electric field on the axis of the gun is the same to within 1% in every cell. Moreover, in the last cell, the symmetry is obviously broken by the presence of the couplers. Nevertheless the field varies by only 1.3 % over a distance equal to 3 times the rms width (about 2 mm) of the beam where 99.7 % of the particles are located.

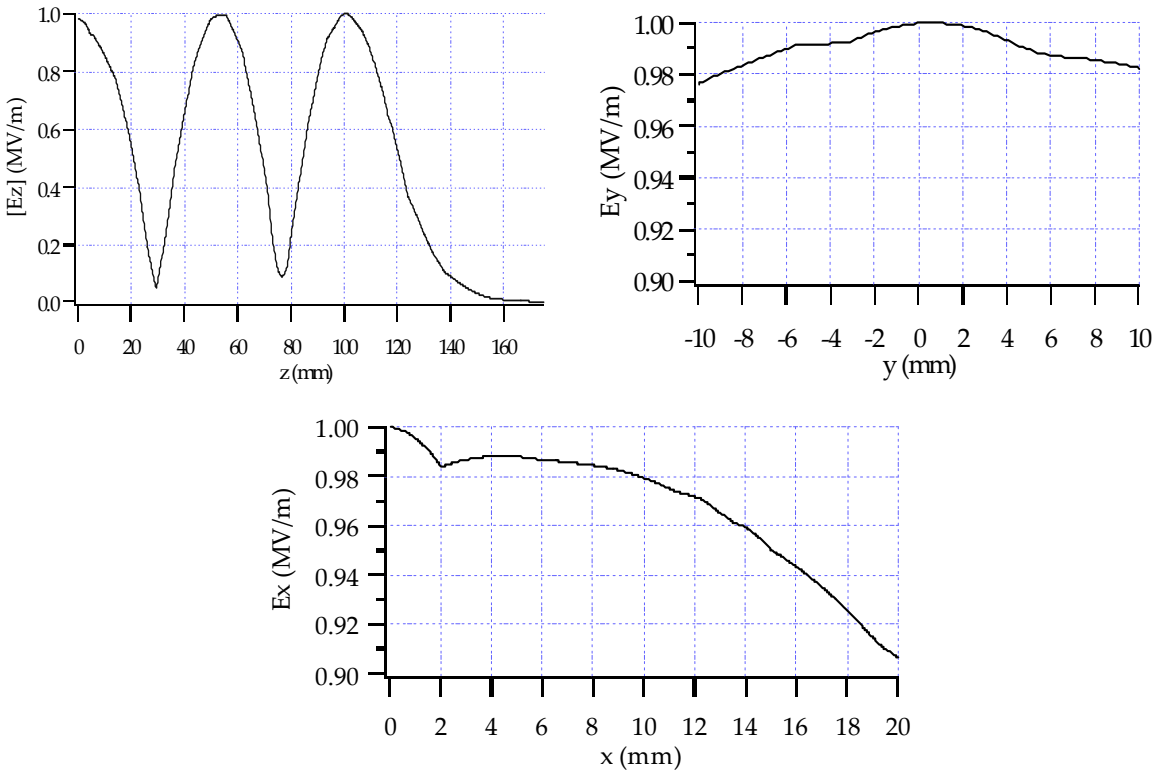

Figure 7: Normalized amplitude of the electric field as a function of the longitudinal axis of the gun. Above left - axial electric field; Above right and lower - the electric field of the last cell versus the vertical axis and horizontal axis, respectively. The zero corresponds to the centre of the cell.

The coupling can be deduced from the width, Δf, at $1/\sqrt{2}$ of the curve of the S_{21}.

$Q_L = \frac{f_r}{\Delta f}$ where Q_L is the loaded quality factor which is related to the Q_0 by:

$Q_L = \frac{Q_0}{1+\beta_T}$ where β_T is the total coupling of the RF photo-gun.

The width is around 0.86 MHz and, assuming a Q_0 = 14500 (the SUPERFISH value is more accurate than that of HFSS), the coupling is 3.1. This value is slightly higher than the required one but in any we will not begin construction of the photo-injector with the final dimensions found with HFSS. We prefer to take an initial error margin around 1 mm and to get the required values of frequency, field and coupling by successive careful mechanical adjustments.

2. Beam dynamics

The simulations with PARMELA presented in this chapter are based on the real longitudinal electric field calculated with SUPERFISH for the 2D model shown in figure 2. Unfortunately, it is not possible to extract the electric field of the HFSS model and to use it in PARMELA.

Several aspects of the beam dynamics have been investigated. First, calculations on the gun alone will be presented. Then, a study of the compensation of the beam emittance increase due to the space charge forces will be presented. The last simulations show what happens when one adds the CERN accelerating section foreseen to be used downstream of the gun.

2.1 RF photo-gun alone

The CERN design of the RF gun was optimised for higher charge (e.g. choice of the angle of the wall around the photo-cathode). Therefore, we decided to study the influence of this parameter on the beam dynamics. The results are summarised in table 3.

	0°	**3.4°**	**8.3°**
σ_x (mm)	3.4	3.25	3.04
ε_T (π mm-mrad)	20.6	20.7	22.3
σ_z (mm)	1.11	1.15	1.2
$\frac{\Delta p}{p}$ (%)	0.6	0.75	2.6

Table 3: results of the simulations with PARMELA with 600 particles and the nominal current of CTF3 (3.51 A) as a function of the wall-angle around the photo-cathode. The widths are rms values and the rms emittance ε_T is normalised.

The case of an angle of 8.3° is incompatible with the gun specifications and the case of 3.4° seems less interesting with respect to a vertical wall. However, with a higher current, a small wall-angle is advantageous as it adds a focusing force which compensates the increase of the space charge forces. So, as we want to maintain the possibility of operating at a higher current, we decided to adopt this small angle on the photo-cathode wall.

Results of the simulations for the gun model shown in Fig. 2 are illustrated in Fig. 8. The beam parameters are summarised in table 4.

E (MeV)	5.452
ε_x (πmmmrad)	19.6
σ_x (mm)	3.2
σ_z (mm)	1.07
$\frac{\sigma_y}{\gamma}$ (%)	0.36

Table 4 : Beam parameters for a beam current I = 3.51 A and a laser spot σ_r = 1.4 mm (rms).

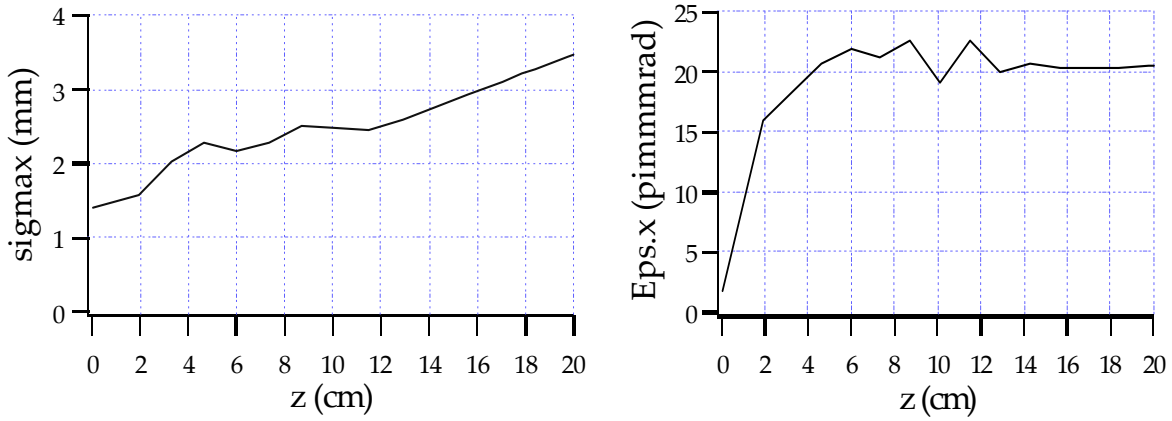

Figure 8: left - horizontal rms width: Right - horizontal normalized emittance.

Every simulation is done with 600 macro-particles, the results are only shown in the x direction because of the cylindrical symmetry and generally there are zero losses in the gun.

The performances of the gun as a function of the shape of the accelerating electric field have been investigated and are illustrated in figure 9. The emittance, in the case of an electric field well balanced in every cell, is lower than in other cases and in addition the peak electric field is lower, for the same average value thus reducing breakdown hazards.

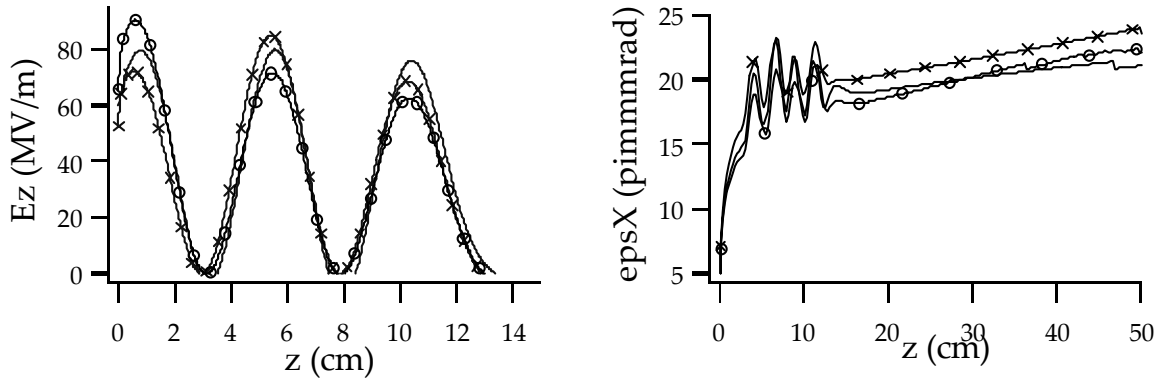

Figure 9: left - electric field as a function of the longitudinal axis of the gun: Right - emittance in x direction as a function of z for 3 cases: full curve, balanced field; curve with circles, strong field in the first cell; curve with crosses, strong field in the second cell.

Simulations have been also done for different laser spot sizes. The results are compiled in Table 5. It would seem more interesting to use a laser spot size smaller than 1 mm as the emittance is significantly lower than in previous calculations done with 1.4 mm. In addition, the bunch length and the energy spread stay within the required limits. Nevertheless, there are some particle losses in the 1st mm after the photo-cathode. We believe the origin of these losses is the strong increase of the space charge which prevents the particles from being extracted. The only solution would be a bigger accelerating voltage in the RF photo-gun.

σ_{laser} (mm)	0.6	0.8	1	1.4	2.8
Particle losses (%)	1	0.3	0.3	0	0
σ_x (mm)	3.16	2.96	2.92	3.22	4.85
ε_x (πmmmrad)	13.5	16	17.6	19.6	21.06
Bunch length (ps)	11	9.6	9	8.4	7.9
σ_γ/γ (%)	0.5	0.4	0.4	0.36	0.41

Table 5: Beam parameters as a function of the laser spot size on the photo-cathode.

2.2 Compensation of the space charge forces

Due to the space charge forces, the emittance grows linearly with the distance until the beam enters the accelerating section. At the output, the emittance is "frozen" because the space charge forces are strongly reduced at high energy. Therefore, to keep the emittance at the lowest possible value, it is necessary to use a transverse focusing between the output of the gun and the input of the section to compensate the defocusing effect of the space charge. One possible technique, proposed by E. Carlsten, is the use of a magnetic lens.

Simulations have been performed with a SLAC type section at the nominal current and 1.4 mm of laser spot size and with two coils for which the positions and the intensity of the field are variable (see figure 10). The fact that we used a SLAC section in the simulations has no influence on the conclusions which can be drawn from this study.

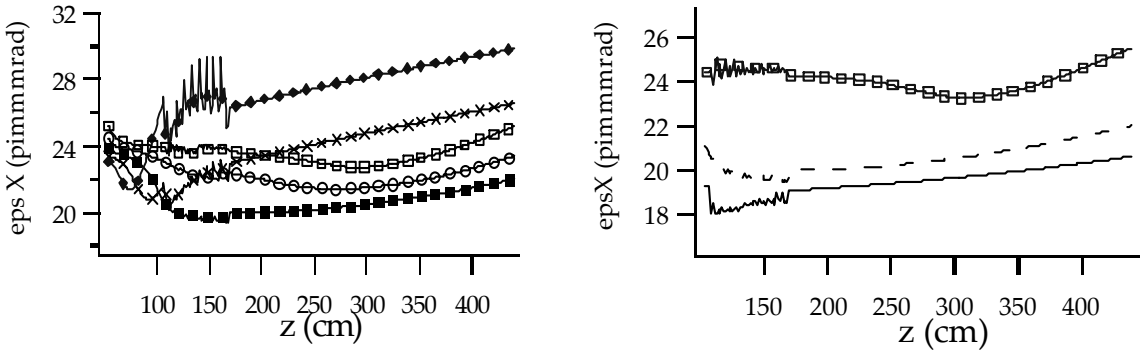

Figure 10: Emittance as a function of distance for several kinds of magnetic field. The SLAC section is located at z = 107 cm and has a length of 63 cm and a gradient of 30 MV/m. Left figure; variable magnetic field, ■, B_z = 0.23 T; ○, B_z = 0.22 T; □, B_z = 0.21 T; X, B_z = 0.24 T; ◆, B_z = 0.25 T. Right fig; variable position of the coils, □, coil at z = 15 cm and B_z = 0.21 T; dashed line, 2 coils at z = 10 cm and 20 cm and B_z = 0.23 T; plain line, 2 coils at z = 2 cm and 10 cm and B_z = 0.25 T. In all cases, thanks to a bucking coil, the magnetic field is less than one gauss on the photo-cathode.

Two important facts can be quoted about the curves in figure 10. There is an optimum value of the magnetic field, 0.23 T for two coils at z = 10&20 cm, for a good compensation of the emittance. But, mainly, it seems that the biggest reduction of the emittance is obtained when the coils are placed near the photo-cathode. With a solenoid ranging from 2 cm to 10

cm and a peak magnetic field of 0.25 T, the emittance is 19 π mm-mrad. This result explains why we choose to connect the couplers to the last cell of the gun in order to leave enough space to install a solenoid.

2.3. Simulations with the real accelerating section

After the study with a SLAC type accelerating section, the results must be validated using a true CERN section. The design of the latter is rather special since it is operated in the so-called "fully-loaded" mode. It means that all the RF power is extracted by the electron beam by the end of the section. A plot of the accelerating field is shown in Fig. 11. The gradient and the iris aperture decrease over the length of the section.

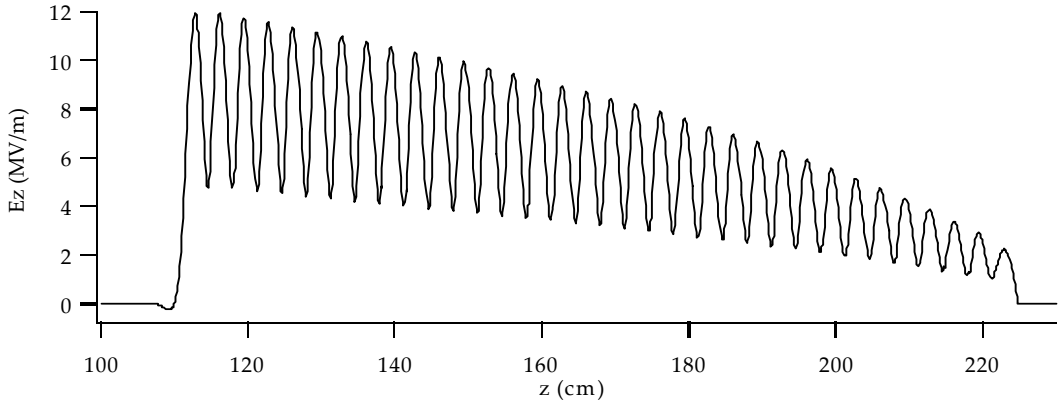

Figure 11: Electric field of one fully-loaded CERN section at I = 3.51 A.

Simulations have been performed taking into account the previous results with the SLAC section, i.e. we assume that the solenoid on the gun is the best condition to have good emittance compensation. The results are shown in Fig. 12.

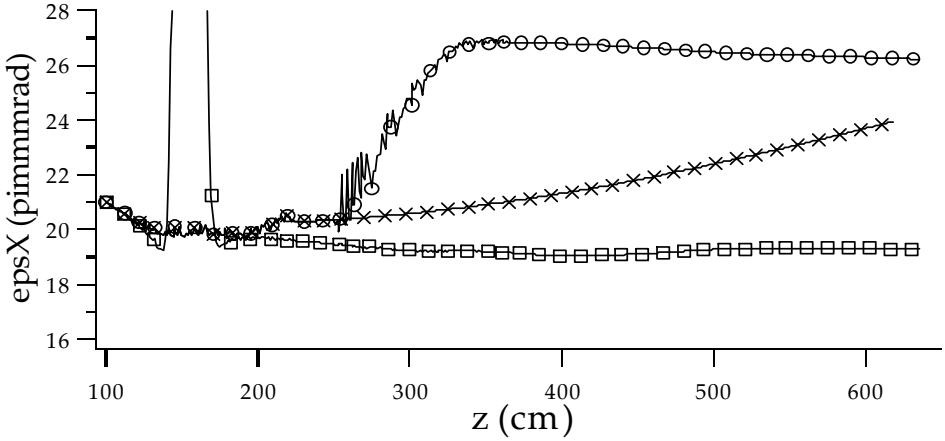

Figure 12: emittance versus distance; line with ○, two CERN sections, the 2nd beginning at 250 cm; line with x's, only one section; line with □'s, coil at z = 150 cm and B_z = 0.13 T

Strangely, we observe that when a 2nd CERN section is used, the emittance undergoes a rapid increase of 30 % while there is only a slight growth due to the residual space charge

forces without the 2nd CERN section. Nevertheless, we are quite confident that this is not an artefact of the simulations as we thoroughly checked the input file and the electric field used in PARMELA. If one applies a magnetic field around the 1st accelerating section the consequence is an emittance effectively reduced to 19.3 π mm-mrad at the exit of the 2nd CERN section. Therefore it seems that the transverse beam quality is degraded in the CERN section. This result is not well understood and hence the results can not be trusted without a more complete study.

3. Beam-Loading

It is well known that the electron beam interacting with the impedance of the RF structures induces a beam loading voltage which can be detrimental for gun operation. Therefore, it is necessary to evaluate this effect quantitatively. The beam loading voltage V_{ind}, after an exponential growth reaches a saturated value, V_{sat}:

$$V_{ind}(t) = V_{sat}(1 - \exp(-\frac{t}{\tau}))$$

$$V_{sat} = \frac{R_s T^2 I_{harm}}{(1+\beta)}$$

$$\tau = \frac{2Q_c}{\omega_r}$$

(1)

where R_s is the shunt impedance, T, the transit time factor, I_{harm}, the 3 GHz component of the beam current and β is the coupling of the gun. Equation 1 can be simplified if one considers that the bunches are short with respect to the RF period, hence $I_{harm} \approx 2I_0$ with I_0 the average current in the train. The value of the parameters that we have used are given in Tables 1, 2 and 4. The peak electric field is 85 MV/m, hence the energy gain would be 14.4 MeV but in PARMELA, we found 5.45 MeV because it includes the slippage of the beam with respect to the RF phase. Therefore, the transit time factor is T = 0.38. At the steady state, β = 1, then the beam loading voltage is $V_{sat} \approx 3$ MV and the induced electric field is 17.7 MV/m. It means that the beam would see a gradient changing from 85 MV/m down to 67 MV/m at the end of the pulse train. To avoid the resulting energy spread, one needs to inject the beam during the rise time of the electric field as described in Fig. 13. In this way, the induced voltage is compensated by the increase of the RF input power resulting in a constant accelerating voltage.

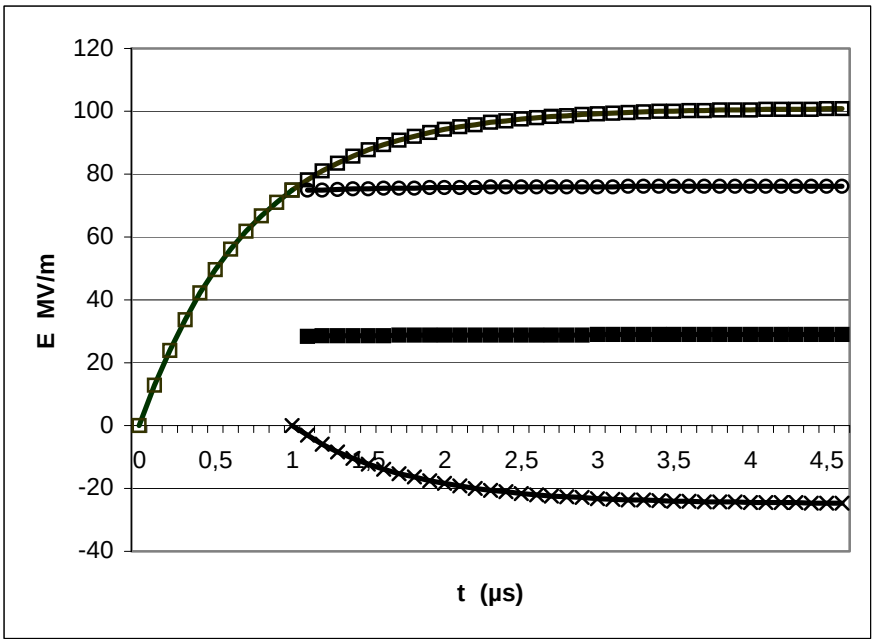

Figure 13: Principal of the beam loading compensation; curves of the electric field in the RF gun: blue, without electron beam; around 1 µs the beam is injected, □, electric field produced by the input RF, x, the beam loading voltage, ○, the difference between both and ■ the accelerating voltage seen by the particle.

In order to compensate the beam loading, the RF input power must be sufficient to create a vacuum peak gradient about 103 MV/m. For our model, the peak electric field is two times bigger than the average value. The latter can be evaluated with:

$$P=\frac{V^2}{Rs} \qquad (2)$$

The required power is then about 13.5 MW, depending on the beam current. If the beam current is higher, 5 A for instance, the beam loading electric field is 25.2 MV/m. Hence, the vacuum electric field must be 110 MV/ and therefore one needs about 16 MW of input power.

Note that we neglected the detuning induced by the beam loading. This detuning depends linearly on sin(ϕ), where ϕ is the phase difference between the electron bunch and the crest of the RF wave, To get the maximum energy out of the RF gun, the particles are on the crest except in the half-cell where there is a phase shift due to the non relativistic velocity of the electrons. As this occurs in the very first part of the structure, it can be probably neglected. In any case, the tuning of the resonant frequency will be possible thanks to the cooling water control.

An important issue to consider is the matching of the RF photo-injector. The reflection factor depends on the coupling, β. In presence of the electron beam, the coupling is given by:

$$\beta = \frac{\beta_0}{1 + \frac{P_{beam}}{P_{RF}}} \qquad (3)$$

where β_0 is the vacuum cavity coupling, P_{RF} is the input RF power and $P_{beam} = VI$ is the power of the electron beam at the output of the RF gun.

For the nominal current, P_{RF} = 13.5 MW and P_{beam} = 19.13 MW. Therefore, to get β = 1 and no reflection in presence of the beam, the RF gun must be over-coupled with β_0 = 2.4. At I = 5 A, β_0 = 2.7, hence it could be convenient to choose an intermediate value to minimize the reflected power over the whole current range.

4. Vacuum Calculations

Vacuum considerations are a critical aspect of the project as the results of experiments performed at CERN have shown an exponential growth of the pressure inside the gun as a function of the total extracted charge, whatever the bunch-train distribution. Therefore, we have started simulations to understand how we can reduce the pressure in the RF photo-gun. A simplified model of the gun, Fig. 14, is used in the MONTE-CARLO based calculations.

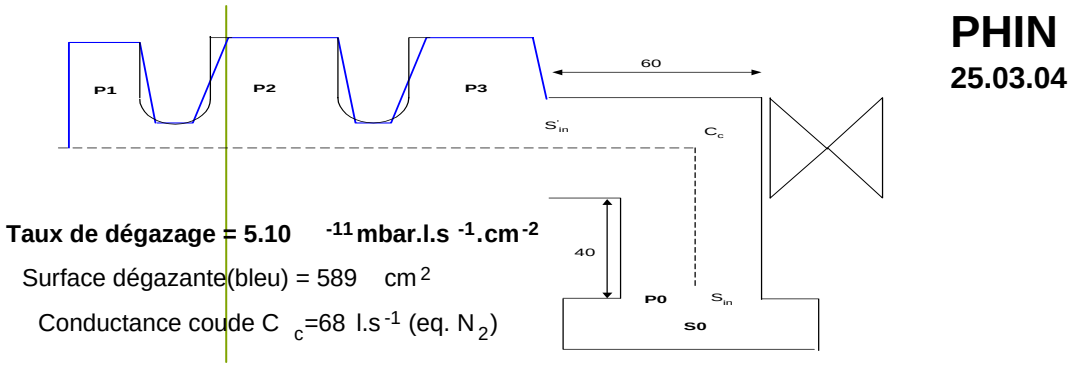

Figure 14: Model of the RF gun for the vacuum calculations, pumping at the exit.

In the simulations, the out-gassing rate for the OFHC copper is assumed to be 5.10^{-11} mbar.l.s^{-1}.cm^{-2} (N_2 equivalent) for a standard cleaning and about one hundred hours of pumping. The residual pressure in the three cells is represented in figure 15.

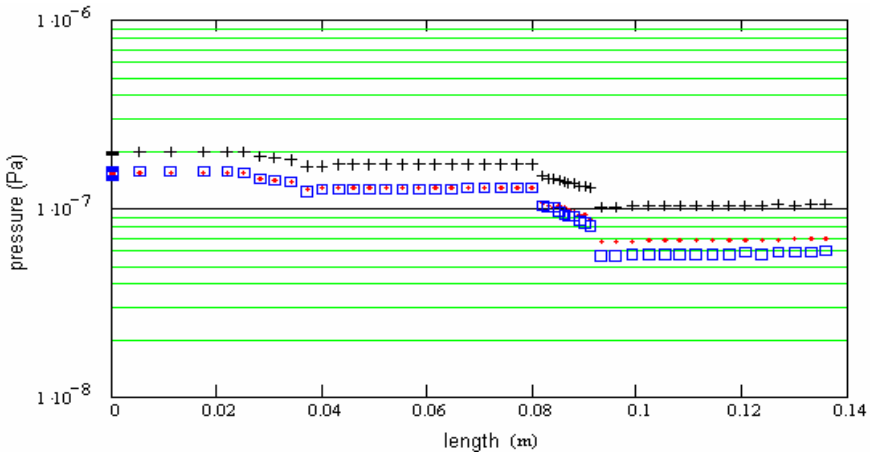

Figure 15: Residual pressure in the gun for 3 pumping speeds: +, 40 l/s; •, 75 l/s; □, 148 l/s.

The average value is 10^{-9} mbar. The pressure is obviously lower in the last part of the RF gun due to the proximity of the pump. In figure 16, the evolution of the pressure in the three cells as a function of the pumping speed shows that it is of no interest to exceed 40 l/s since the pressure does not improve significantly above this speed.

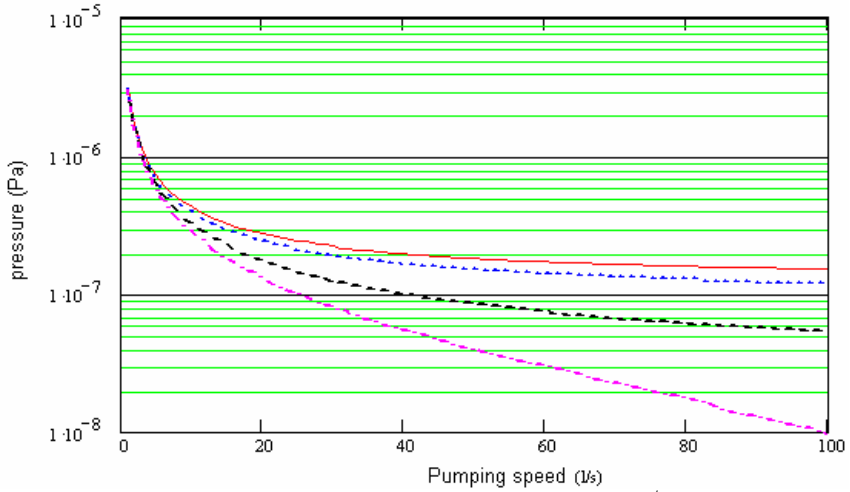

Figure 16 : Pressure as a function of the pumping speed in: the 1st cell (plain line), the 2nd cell (thin dashed line), the 3rd cell (thick dashed line). The lowest curve corresponds to the pressure in front of the pump.

The influence of supplementary pumping through the RF input coupling apertures is shown in Fig. 17. The pumping speed employed, 20 l/s, is quite modest because the coupling holes are, in general, small.

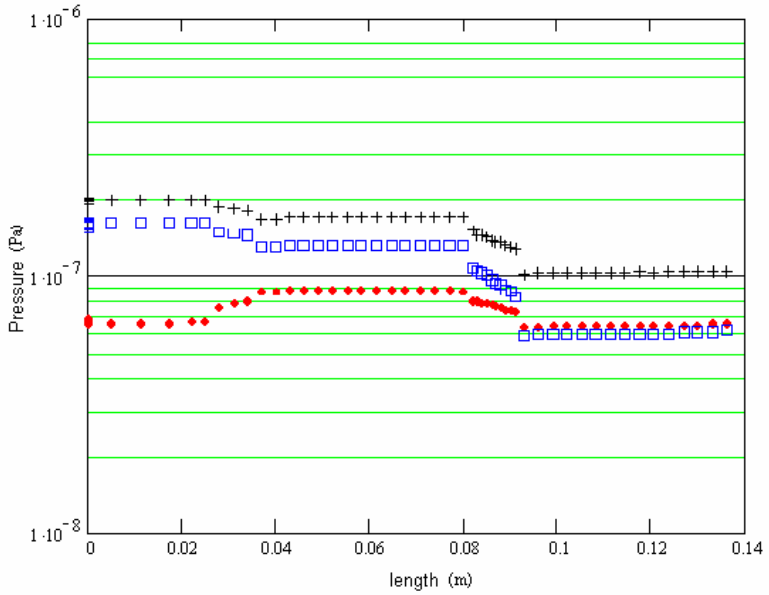

Figure 17: Pressure along the RF photo-injector; +, no additional pumping; •, pumping in the 1st cell; □, pumping in the 3rd cell.

On the one hand, pumping in the 1st cell would reduce the pressure by 3 and, on the other hand, the reduction is negligible compared to pumping in the 3rd cell. Unfortunately, there is no choice other than to connect the RF wave-guides to the 3rd cell, as discussed above. Hence, to really reduce the pressure it is crucial to lower the out-gassing rate of the copper. One solution is a high temperature bake of the photo-injector. In this case, calculations predict a residual pressure of 10^{-11} mbar in the 1st cell.

Conclusion

The design of the RF photo-injector is almost completed. It still needs further simulations for the shape of the last cell to improve the electric field symmetry. Tolerances remain to be defined and the implied changes of the shape must be compatible with mechanical issues. However, with the present model, electron beam dynamic simulations have been performed and have shown that one can fulfill the CTF3 requirements. An increase of the beam emittance due to an effect of the CERN accelerating section is observed unless the beam radius is reduced by the use of a solenoid. This phenomenon is puzzling and needs further investigation. The beam-loading induced by the beam is quite manageable, even at a higher current than the nominal one. The vacuum issue gives cause fore concern as the simulations show the pumping speed is limited by the weak conductance of the RF gun. Basically, there will be two major differences compared with the previous CERN arrangement: a pump at the exit of the gun and a high temperature bake-out.